A Simple Model of the Decadal Response of the Ocean to Stochastic Wind Forcing*

CLAUDE FRANKIGNOUL

*Laboratoire d'Océanographie Dynamique et de Climatologie, Unité Mixte de Recherche CNRS–ORSTOM–UPMC,
Université Pierre et Marie Curie, Paris, France*

PETER MÜLLER

Department of Oceanography, University of Hawaii, Honolulu, Hawaii

EDUARDO ZORITA[+]

Laboratoire d'Océanographie Dynamique et de Climatologie, Université Pierre et Marie Curie, Paris, France

(Manuscript received 15 May 1996, in final form 15 October 1996)

ABSTRACT

A simple linear model is used to estimate the decadal response of the extratropical ocean to wind stress forcing, assuming a flat bottom, a mean state at rest, and no dissipation. The barotropic fields are governed by a time-dependent Sverdrup balance, the baroclinic ones by the long Rossby wave equation. The ocean is bounded by a coast in the east and a radiation condition is used in the west. At each frequency, the baroclinic response consists of a forced response plus a Rossby wave generated at the eastern boundary. For zonally independent forcing, the response propagates westward at twice the Rossby phase speed. The wind stress is assumed to be stochastic with a white frequency spectrum, so the model represents the continuous excitation of the ocean interior by the weather fluctuations. The model predicts the shape and level of the frequency spectra of the oceanic pressure field and their variation with longitude and latitude. The baroclinic response is spread over a continuum of frequencies, with a dominant timescale determined by the time it takes a long baroclinic Rossby wave to propagate across the basin and thus increases with the basin width.

The predictions for zonally independent forcing are compared with the North Atlantic pressure variability in an extended integration of the ECHAM1/LSG coupled GCM. The agreement is good in the interior of the subtropical gyre, but less satisfactory in the subpolar gyre. The theory correctly predicts that the baroclinic spectra are red with a high-frequency ω^{-2} decay that levels off at low frequency, and how this spectral shape changes with longitude as a result of varying fetch and with latitude as a result of parameter changes. The theory predicts that the barotropic frequency spectra are white, whereas the GCM spectra are slightly red. Nevertheless, it captures how the barotropic pressure spectra vary with longitude, latitude, and wind stress intensity. The baroclinic predictions for a white wind stress curl spectrum are also broadly consistent with the frequency spectrum of sea level changes and temperature fluctuations in the thermocline observed near Bermuda. Stochastic wind stress forcing may thus explain a substantial part of the decadal variability of the oceanic gyre.

1. Introduction

There is increasing observational evidence of the decadal variability of the extratropical oceans. In particular, Bjerknes (1964), Deser and Blackmon (1993), and

[+] Current affiliation: GKSS-Forschungszentrum Geesthacht, Insitut für Gewässerphysik, Geesthacht, Germany.

Corresponding author address: Dr. Claude Frankignoul, LODYC/ CNRS–ORSTOM–UPMC, Universite Pierre et Marie Curie, 4 Place Jussieu, 75005 Paris, France
E-mail: cf@lodyc.jussieu.fr

Kushnir (1994) have investigated the low-frequency variability of the sea surface temperature (SST) in the North Atlantic and its relation to the atmosphere, suggesting that there were two different modes of variability: decadal SST changes with a dipole pattern and a dominant period of about 10–15 years, which seemed to be driven by air–sea flux variations, and "interdecadal" basin-scale fluctuations with a dominant period of perhaps 40–50 years, which seemed to be linked to changes in the large-scale oceanic thermohaline circulation and to different phases of the North Atlantic Oscillation. Changes corresponding to the interdecadal mode were detected by Levitus (1989) in hydrographic observations of the upper 1000 m of the ocean, while decadal fluctuations opposite in phase in the subtropical and subpolar gyres were found in the upper-ocean temperature by Levitus et al. (1994). Near Bermuda, Joyce

and Robbins (1996) found in-phase decadal changes of temperature and salinity in the thermocline, which could be explained by large vertical or meridional displacements, and interdecadal changes at larger depths. Decadal variability was also seen in the Bermuda tide gauge record analyzed by Sturges and Hong (1995), who showed that the sea level changes could be explained by the baroclinic oceanic response to wind stress forcing across the Atlantic. In the Pacific, the role played by ENSO and its teleconnection with the extratropical atmospheric and oceanic circulation has been stressed by Trenberth and Hurrel (1994) and Graham (1994), whereas Zhang et al. (1996) suggested that the midlatitude variability was only partly forced from the Tropics. Decadal variations in the Alaska gyre were investigated by Lagerloef (1995) and interpreted as a stochastically forced variability primarily due to Ekman pumping.

Experiments made with coupled ocean–atmosphere general circulation models (GCMs) provide a more complete view of the decadal changes but, because of computational cost, model resolution has been limited, the physics oversimplified, and flux corrections often applied to avoid climate drift; so the results must be considered with caution. In a 600-yr integration of the Geophysical Fluid Dynamic Laboratory low-resolution coupled GCM, Delworth et al. (1993) found that the interaction between the thermohaline and the gyre circulations in the North Atlantic could generate self-sustained oscillations in the 50-yr timescale, characterized by a lag between temperature and salinity changes; the atmosphere seemed to play little role. Based on a shorter experiment with the higher-resolution ECHO coupled GCM developed at the Max-Planck-Institut für Meteorologie in Hamburg (MPI), Latif and Barnett (1994) suggested that a substantial decadal variability with a period of about 20 years resulted from feedbacks between changes in the subtropical gyre and the atmosphere in the North Pacific: an anomalously strong subtropical gyre caused higher SSTs at mid latitudes, which gave rise to an enhanced surface heating that reinforced the SST anomaly, but also to a weaker Aleutian low, weaker zonal winds, and, after a lag related to the gyre adjustment time, a weaker subtropical gyre; so the cycle repeated with the reversed sign. In a 325-yr integration with the low-resolution MPI ECHAM1/LSG coupled GCM, von Storch (1994) found decadal changes in the whole Pacific Ocean, even though there was no ENSO in the model, which involved changes in the intensity of the Pacific subtropical gyres via Rossby wave propagation and advection of oceanic disturbances. Robertson (1996) has suggested that in the North Pacific, the mode was forced by air–sea interactions. In the ECHAM1/LSG simulation, the decadal variability in the North Atlantic was investigated by Zorita and Frankignoul (1997). Although the fluctuations formed a continuum of frequencies, two distinct modes of ocean–atmosphere variability were identified, with the oceanic changes reflecting the atmospheric forcing through anomalous air–sea fluxes and Ekman pumping, which after some delay affected the intensity of the subtropical and subpolar gyres. The most energetic mode had a dominant period of about 20 years and seemed to reflect a passive oceanic response. The other mode with a 10-yr period was speculated to be a coupled mode involving air–sea feedbacks.

In summary, there seem to be two different modes of low-frequency variability: a decadal variability that appears to be linked to the atmospheric forcing and an interdecadal one that seems to be of oceanic origin. Whether or not the ocean is only passive on the decadal scale has not been established from the limited observational record, while both active and passive behaviors have been suggested by the coupled GCM experiments. Also, the mechanisms that determine the vertical structure and the dominant timescale of the fluctuations have not been clearly identified. This points to a need for basic studies of the ocean–atmosphere interactions on the decadal scale.

In the present paper, we try to establish how much of the decadal variability of the extratropical oceanic pressure field can be explained by their passive response to stochastic wind stress forcing, that is, to the day-to-day changes that are associated with the weather fluctuations. This can be viewed as the simplest model of the decadal variability of the ocean, since it does not involve its back interaction onto the atmosphere, and it provides a reasonable null hypothesis that should be considered when testing more elaborate models based on an active ocean. Since the seminal paper of Hasselmann (1976), stochastic climate models have been applied to SST anomalies, sea ice fluctuations, soil moisture changes, oceanic quasigeostrophic fluctuations, as well as to longer timescale changes involving the thermohaline circulation and the dynamics of the whole climate system [see Frankignoul (1995) for a recent review]. Here, the concept is applied to the low-frequency variability of the wind-driven circulation.

Because of the complexity of the oceanic circulation, the problem of its response to fluctuating forcing is formidable. Even studies that do not consider the western boundary current dynamics can become very intricate when the oceanic basic state is nonuniform, as in Liu (1993), and are of limited use for quantitative assessments. Thus, we choose the simplest possible oceanic model that can answer our zeroth-order question, namely whether the magnitude of the response of the ocean interior to stochastic wind forcing is comparable to that of the observations: a linear, flat-bottom, two-mode or two-layer model with a basic state at rest. Western boundary dynamics are not considered, nor are frictional processes; hence many details of the oceanic signal are not expected to be reproduced. On the other hand, the model is simple enough to calculate the oceanic response spectrum to a realistic atmospheric forcing spectrum, providing statistical signatures like its zonal and

meridional dependences, which can be compared to observations in regions where it approximately applies.

In section 2, we discuss our simple model of the decadal oceanic response to stochastic wind forcing. As the observations are limited, we compare in section 3 our theoretical predictions to the decadal pressure variability found in the North Atlantic in the ECHAM1/LSG coupled GCM. This variability has been investigated by Zorita and Frankignoul (1997) and a discussion of their results is given in light of our theory. Observational data at Bermuda are discussed in section 4, and conclusions given in section 5.

2. The oceanic model

As the simplest ocean model we choose a linear, ideal fluid, planetary geostrophic model with a basic state at rest. The effects of mean flow and thermocline structure are not considered. A no-normal flow condition is imposed at the eastern boundary and a radiation condition in the west. Western boundary dynamics are excluded; hence the model only applies east of the western boundary current regions. The bottom is assumed to be flat. The only forcing is the surface wind stress transmitted to the ocean by Ekman pumping. The forcing by buoyancy fluxes and freshwater exchanges is not considered, nor that by the atmospheric pressure, and sea surface temperature variations are not discussed. The governing equations are the time-dependent Sverdrup balance for the barotropic response and the forced long-wave equation for the baroclinic one.

The time-dependent Sverdrup balance is given by

$$\frac{\beta}{a\,\cos\theta}\frac{\partial p_{bt}}{\partial\varphi} = \frac{\rho f^2}{H}w_e \quad \text{or} \quad \beta v_{bt} = \frac{f}{H}w_e, \qquad (1)$$

where p_{bt} is the barotropic pressure, v_{bt} the barotropic meridional velocity, φ the longitude, θ the latitude, a the radius of the earth, $f = 2\Omega\sin\theta$ the Coriolis parameter, β the meridional gradient of the Coriolis parameter, and H the ocean depth. The Ekman velocity is given by

$$w_e = \frac{1}{\rho}\left(\boldsymbol{\nabla}\times\frac{\boldsymbol{\tau}}{f}\right) \qquad (2)$$

in terms of the atmospheric wind stress τ. The balance (1) states that the input of vorticity by the wind is immediately balanced by a change in planetary vorticity. This neglects the time-dependent adjustment process by barotropic Rossby waves, which happens on timescales of a few days and can be considered infinitesimal on the decadal timescale considered here. The influence of topography and the joint effect of baroclinicity and bottom relief (JEBAR) have been eliminated by our assumption of a flat bottom.

The baroclinic pressure at depth z is given by $p_{bc}(\varphi, \theta, t)\,\phi(z)$, where $\phi(z)$ is normalized in a depth-averaged sense by setting $\int_{-H}^{0}\phi^2(z)\,dz = H$. The evolution equation for p_{bc} can be written

$$\frac{\partial p_{bc}}{\partial t} + c_{bc}\frac{1}{a\,\cos\theta}\frac{\partial p_{bc}}{\partial\varphi} = -\frac{\rho f^2}{H_{bc}}R_{bc}^2 w_e, \qquad (3)$$

where R_{bc} is the deformation radius and $c_{bc} = -\beta R_{bc}^2$ the zonal phase speed of the long, nondispersive Rossby waves. Here H_{bc} is a baroclinic depth scale that depends on the stratification. In a continuously stratified model we identify the baroclinic response with the first mode of the infinite set of baroclinic modes. Then, one has $H_{bc} = H/\phi(0)$, where $\phi(0)$ is the value of the first baroclinic eigenfunction $\phi(z)$ at the surface. For $H = 4500$ m and $\phi(0) = 3$ as representative of the region near 28°N, 70°W one obtains a baroclinic depth scale $H_{bc} = 1500$ m. In a two-layer model, $H_{bc} = (H_1/H_2)^{1/2}\,H$, where H_1 and H_2 are the upper and lower layer thicknesses. To obtain the same baroclinic depth scale one has to choose $H_1 \approx 500$ m. Higher baroclinic modes are assumed to be less important and are not considered.

Equations (1)–(3) are very simple, and latitude enters as a parameter only. The response can therefore be calculated for every latitude separately with the appropriate values of f, β, R_{bc}, $\phi(z)$, H, and H_{bc}. The dependence on θ will be dropped and $x = \varphi a\cos\theta$ used as the zonal coordinate.

The lateral domain is a half-plane with an eastern boundary. The kinematic boundary condition of no-normal flow at the eastern boundary implies (via the geostrophic relation) that the pressures p_{bt} and p_{bc} at the boundary are functions of time at most. This function is set to zero. The general solution with this boundary condition is

$$p_{bt}(x, t) = \frac{1}{\beta}\int_0^x dx'\,F(x', t) \quad \text{or}$$

$$v_{bt}(x, t) = \frac{1}{\rho f\beta}F(x, t) \qquad (4)$$

$$p_{bc}(x, t) = \frac{H}{\beta H_{bc}}\int_0^x dx'\,F\left(x', t - \frac{x - x'}{c_{bc}}\right) \qquad (5)$$

with the forcing function

$$F = \frac{\rho f^2}{H}w_e.$$

Note that the baroclinic response does not depend on the ocean depth H but only on the baroclinic depth scale H_{bc}. Fourier transformation in time leads to the following relations between the Fourier components of the forcing and the response

$$\hat{p}_{bt}(x, \omega) = \frac{1}{\beta}\int_0^x dx'\,\hat{F}(x', \omega) \quad \text{or}$$

$$\hat{v}_{bt}(x, \omega) = \frac{1}{\rho f\beta}\hat{F}(x, \omega) \qquad (6)$$

$$\hat{p}_{bc}(x, \omega) = \frac{H}{\beta H_{bc}}\int_0^x dx'\,\hat{F}(x', \omega)e^{ik_{bc}(x-x')}, \qquad (7)$$

where

$$k_{bc} = \frac{\omega}{c_{bc}} = -\frac{\omega}{\beta R_{bc}^2} \qquad (8)$$

and ω is the frequency. As a further simplification we assume that the wind stress curl and hence the forcing function F are zonally independent. The solution is then

$$\hat{p}_{bt}(x, \omega) = \frac{x}{\beta}\hat{F}(\omega) \qquad (9)$$

$$\hat{p}_{bc}(x, \omega) = \frac{H}{\beta H_{bc}}\frac{1}{ik_{bc}}(e^{ik_{bc}x} - 1)\hat{F}(\omega). \qquad (10)$$

Note that the response is x-dependent although the forcing is not. In the barotropic case this is a consequence of our use of pressure as a variable; the meridional velocity is x-independent. In the baroclinic case, however, the response consists of a directly forced x-independent part to which a free Rossby wave is added to satisfy the boundary condition at the eastern boundary. Hereafter we will call the former the local response and the latter the remote response. The zonal wavenumber of the free Rossby wave, k_{bc}, satisfies the dispersion relation for long nondispersive Rossby waves. The response to $F(t) = F_0\cos\omega t$ is

$$p_{bc}(x, t) = \frac{2H}{\beta H_{bc}}\frac{F_0}{k_{bc}}\sin\frac{1}{2}k_{bc}x \cos\left(\frac{1}{2}k_{bc}x - \omega t\right), \quad (11)$$

a wave that propagates with a phase speed twice that of the free Rossby wave and whose amplitude is modulated by the factor

$$\frac{1}{k_{bc}}\sin\frac{1}{2}k_{bc}x,$$

which depends on frequency. Relation (11) has been previously derived by White (1977). The modulation reaches its first maximum of $1/k_{bc}$ at a distance $\Delta x = \pi/k_{bc}$ away from the eastern boundary where the local and remote responses become in phase. Note that for very small values of $k_{bc}x$ there is enough time for baroclinic adjustment and p_{bc} increases linearly with x as in (9).

For a two-layer system one can calculate from (9) and (10) the pressure in the upper and lower layers:

$$\hat{p}_1(x, \omega) = \hat{p}_{bt} + \left(\frac{H_2}{H_1}\right)^{1/2}\hat{p}_{bc}$$

$$= \frac{\hat{F}(\omega)}{\beta}\left[x + \frac{H_2}{iH_1 k_{bc}}(e^{ik_{bc}x} - 1)\right] \qquad (12)$$

$$\hat{p}_2(x, \omega) = \hat{p}_{bt} - \left(\frac{H_1}{H_2}\right)^{1/2}\hat{p}_{bc}$$

$$= \frac{\hat{F}(\omega)}{\beta}\left[x - \frac{1}{ik_{bc}}(e^{ik_{bc}x} - 1)\right]. \qquad (13)$$

For small x the lower-layer pressure increases quadratically away from the eastern boundary with a coefficient proportional to k_{bc}. Again, when the frequency of the forcing is low enough—that is, for $\omega \to 0$ and hence $k_{bc} \to 0$, the ocean is baroclinically adjusted and the lower layer remains motionless, a result that has plagued early theories of the wind-driven steady circulation in a stratified ocean.

At each frequency, the baroclinic response propagates westward at twice the Rossby wave speed because of the presence of the eastern boundary and our assumption of zonally independent forcing. This doubling might explain the occurence of phase speeds faster than the phase speed of a free Rossby wave (by a factor of about 2 in extratropical latitudes), which has been noted from upper-ocean thermal data (e.g., White 1985; Kessler 1990) and the TOPEX-POSEIDON altimetric data (Chelton and Schlax 1996).[1]

The assumption of zonally independent forcing has been introduced to obtain maximum simplicity. Zonal dependence of the forcing can be easily added. The baroclinic response to a propagating or standing pattern of wavenumber k is given in the appendix.

We now assume that the forcing is a stationary random process with zero mean. The variance is described by the frequency spectrum $S_F(\omega)$, which is related to the Fourier components by

$$S_F(\omega)\delta(\omega - \omega') = \langle\hat{F}(\omega)\hat{F}^*(\omega')\rangle. \qquad (14)$$

The response is also a stationary random process with zero mean, and the spectra of the barotropic and the baroclinic pressure at depth z are given by

$$S_{bt}(x, \omega) = \frac{x^2}{\beta^2}S_F(\omega) \qquad (15)$$

$$S_{bc}(x, z, \omega) = 4\phi^2(z)\frac{H^2 R_{bc}^4}{H_{bc}^2\omega^2}\frac{1}{2}\left(1 - \cos\frac{\omega x}{\beta R_{bc}^2}\right)S_F(\omega). \qquad (16)$$

We finally assume that the wind stress curl spectrum and hence the forcing spectrum are white in frequency space,

$$S_F(\omega) = S_0, \qquad (17)$$

as suggested by the data discussed below. Then the frequency spectrum of the barotropic pressure is white and increases quadratically away from the eastern boundary. The baroclinic pressure spectrum shows the following features (Fig. 1):

1) a high-frequency -2 slope with level

$$4\phi^2(z)\frac{H^2 R_{bc}^4}{H_{bc}^2\omega^2}S_0$$

that is independent of x

---

[1] *Note added in proof:* Indeed, this frequency doubling has become an important part of a more comprehensive explanation of the observed phase speeds in off-equatorial oceans by Qui et al. (1997).
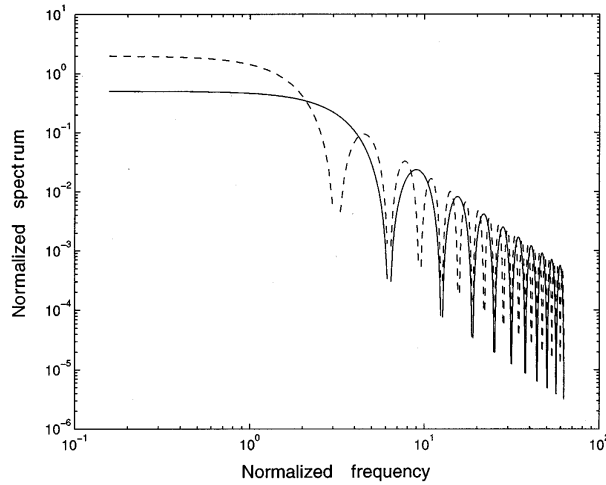
FIG. 1. Normalized spectrum of the baroclinic response as a function of frequency ω/ω' for locations $x = -L$ (solid line) and $x = -2L$ (dashed line). Here $\omega' = R_{bc}{}^2/L$ with an arbitrary length scale L.
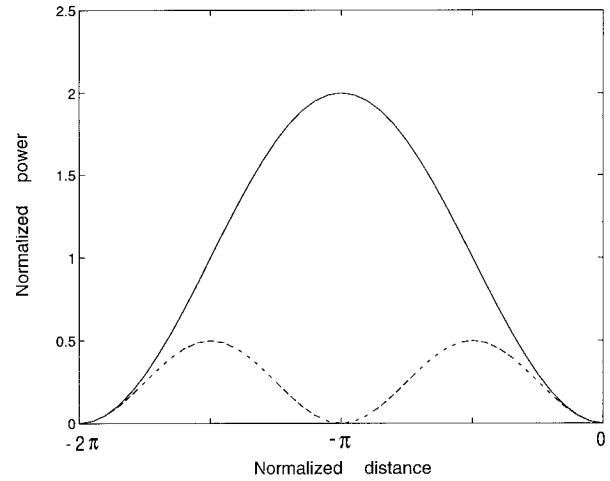

FIG. 2. Normalized power of the baroclinic response as a function of distance x/L for frequencies ω' (solid line) and $2\omega'$ (dashed line), with ω' as in Fig. 1.

2) a modulation

$$\frac{1}{2}\left(1 - \cos\frac{\omega x}{\beta R_{bc}^2}\right)$$

that depends on x

3) a flattening at low frequencies ($\omega \ll 2\pi/\Delta t$) toward a level

$$S_{bc}(\omega = 0) = \phi^2(z)\frac{H^2 R_{bc}^4}{H_{bc}^2}S_0\frac{x^2}{c_{bc}^2}$$

that increases quadratically with the distance from the eastern boundary.

Here $\Delta t = x/c_{bc}$ is the time it takes the nondispersive Rossby wave to travel from the eastern boundary to position x. The spectrum is zero at frequencies $\omega_n = 2n\pi/\Delta t$ and touches the power-law line at $\omega_n = (2n + 1)\pi/\Delta t$, n being a positive integer. Note that we do not expect to see such modulation in observed or GCM data since including x-dependent forcing, adding vertical modes, or considering additional physical processes like friction would all tend to smooth the spectrum.

The x dependence of the baroclinic pressure spectrum

is shown in Fig. 2. For each frequency, the power varies sinusoidally. The spectrum reaches its first maximum of

$$S_{max} = 4\phi^2(z)\frac{H^2 R_{bc}^4}{H_{bc}^2\omega^2}S_0 \tag{18}$$

at a distance

$$\Delta x = \frac{\pi}{k_{bc}} = \frac{\pi\beta R_{bc}^2}{\omega} \tag{19}$$

away from the eastern boundary. The maximum value and the distance Δx increase with decreasing frequency. At the maximum the pressure is in phase quadrature with the Ekman pumping since local and remote responses simply add. At 30°N, Δx is of the order of 3000 km for a period of 10 yr, and 6000 km for 20 years, assuming $R_{bc} = 34$ km (see Table 1). At 45°N the corresponding values are 1000 km and 2000 km for $R_{bc} = 19$ km. The first maximum in the power at a given frequency is not reached if the "effective" width of the basin (its width east of the boundary current region) is smaller than Δx. We do not expect the power to vanish at $2\Delta x$, for the same reasons as above.

The ratio of baroclinic to barotropic response depends

TABLE 1. Standard values for the theoretical predictions.

|	Parameters	Baroclinic mode	Forcing
GCM 30°N	$f = 7 \times 10^{-5}$ s^{-1} $\beta = 2 \times 10^{-11}$ m^{-1} s^{-1} $H = 4500$ m	$H_{bc} = 1500$ m $R_{bc} = 34$ km $\phi(250$ m$) = 2.6$	$S_{curl}(0) = 5 \times 10^{-17}$ Pa^2 m^{-2}/cpy $S_0 = 1.2 \times 10^{-32}$ Pa^2 m^{-4} s^{-2}/cpy
GCM 45°N	$f = 10^{-4}$ s^{-1} $\beta = 1.6 \times 10^{-11}$ m^{-1} s^{-1} $H = 3300$ m	$H_{bc} = 1500$ m $R_{bc} = 19$ km $\phi(250$ m$) = 2.6$	$S_{curl}(0) = 2.5 \times 10^{-16}$ Pa^2 m^{-2}/cpy $S_0 = 1.2 \times 10^{-32}$ Pa^2 m^{-4} s^{-2}/cpy
Bermuda	$f = 8 \times 10^{-5}$ s^{-1} $\beta = 1.9 \times 10^{-11}$ m^{-1}s^{-1} $d\overline{T}/dz = 1.2 \times 10^{-2}$°C/m $N^2 = -(g/\rho)(d\bar{p}/dz) = 10^{-5}$ s^{-2}	$H_{bc} = 1500$ m $R_{bc} = 33$ km $\phi(0) = 3$ $d\phi/dz(500$ m$) = 3/1500$ m	$S_{curl}(0) = 3 \times 10^{-16}$ Pa^2 m^{-2}/cpy $S_0 = 7 \times 10^{-32}$ Pa^2 m^{-4}s^{-2}/cpy
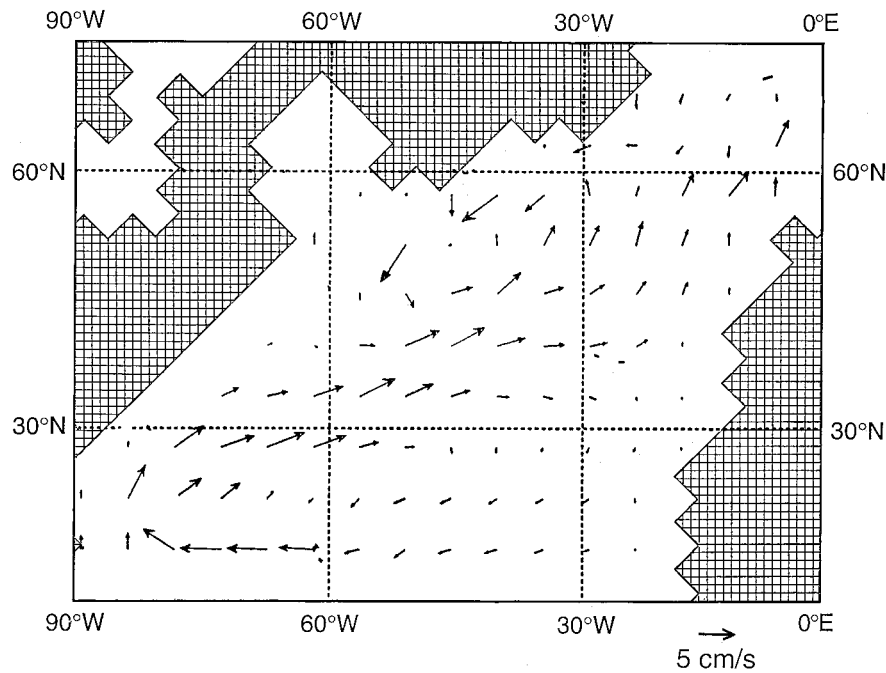
Fig. 3. Horizontal current at 250 m averaged over year 9–708 in the ECHAM1/LSG run.

on both x and ω. However, for $\omega \ll 2\pi/\Delta t$, the ratio is independent of x and given by

$$\frac{S_{bc}(\omega = 0)}{S_{bt}} = \phi^2(z)\frac{H^2}{H_{bc}^2}. \qquad (20)$$

At sufficiently low frequencies, the baroclinic response is always larger than the barotropic one.

All features depend on the meridional coordinate through the parameters H_{bc}, H, β, $\phi(z)$ R_{bc}, and S_0, where the latter two change the most. Note that our model does not predict a response at a specific frequency but a response spread over a continuum of frequencies. However, a dominant timescale or frequency can be associated with the baroclinic response in the same way as a dominant timescale is associated with a first-order Markov process since the spectrum shows a mild bump at a frequency ω^* slightly below $\pi/\Delta t = \pi c_{bc}/x$ when plotted in a variance conserving way [the maximum of ω times (16) is at $2.8/\Delta t$]. This dominant frequency depends on x, decreasing with increasing distance from the eastern boundary. Since the power at ω^* increases quadratically with x, it is the effective width of the basin that sets the frequency that dominates overall, namely ω^* in the western part of the domain. In a larger ocean, both the baroclinic response and its dominant timescale are expected to be larger.

3. Comparison with data from a coupled ocean–atmosphere GCM

a. The ECHAM1/LSG coupled ocean–atmosphere GCM

The model was developed at the Max-Planck-Institut für Meteorologie in Hamburg. The atmospheric com-

ponent is the ECHAM1-T21 model with an equivalent horizontal resolution of about 5.6° × 5.6° and 19 vertical levels (Roeckner et al. 1992). The ocean component is the large-scale geostrophic (LSG) model of Maier-Reimer et al. (1993) with an effective resolution of about 4° × 4° and 11 vertical levels, the first five being at 25, 75, 150, 250, and 450 m, and a smoothed topography. In this primitive equation model, the nonlinear advection of momentum is neglected and an implicit integration scheme used. The free surface is treated prognostically. Sea ice simply appears when the water temperature falls below the freezing point. The atmospheric and oceanic components are coupled synchronously as described in Cubasch et al. (1992), with a large flux correction, given in Gates et al. (1993), to reduce climate drift.

The first 325 years of the integration have been described by von Storch (1994). At the begining, the model is not in equilibrium and there are large changes in sea ice cover, especially in the Southern Hemisphere; the surface temperature first decreases globally, then recovers slowly, but by year 300 the model has reached statistical equilibrium. It was found that the initial adjustment has a negligible influence on the decadal fluctuations of interest here. Hence, we will work with yearly averaged data from year 9 to 708.

Because of a poor simulation of the Icelandic low, the North Atlantic wind stress climatology is not realistic in the coupled model. The zero line of the wind stress curl is located too far south; hence the Gulf Stream and the subtropical gyre are shifted southeastward and the subpolar gyre is too extended. As expected from the
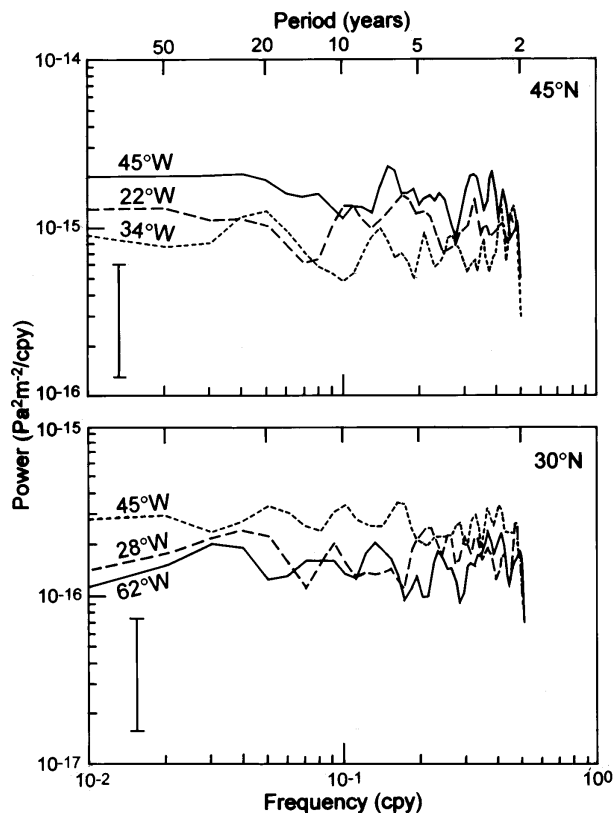
FIG. 4. Frequency spectrum of the ECHAM1/LSG surface wind stress curl at 45°N (top) and 30°N (bottom) and various longitudes. The spectra were estimated from seven independent, detrended 100-yr pieces, from year 9 to 708. The 95% confidence interval is indicated.

low oceanic resolution, the Gulf Stream is also too broad (Fig. 3).

b. Wind stress curl spectrum

Except at the very low frequencies that are affected by the initial model adjustment, the spectrum of the ECHAM1/LSG wind stress curl is essentially white at low frequencies (Fig. 4). In the North Atlantic, its spectral density is about 10^{-15} (Pa m^{-1})^2/cpy at 45°N and 2 10^{-16} (Pa m^{-1})^2/cpy at 30°N, about four times less than in the observations (see below). The white noise level tends to be a bit larger in the center of the basin, but the zonal changes are small. Although the zonal wavenumber spectra estimated from hemispheric data are approximately white, with no significant east–west asymmetry (not shown), an EOF analysis above the North Atlantic domain suggests that the main patterns of wind stress curl variability have zonal scales that are larger than or comparable with the basin width (Fig. 5), with a white frequency spectrum (not shown). Thus, a substantial part of the forcing can be considered to be zonally independent as in the theory. For quantitative comparisons with the model predictions we choose one-quarter of the above values for the stochastic forcing level S_0 (see Table 1).

c. Comparison with the model predictions

For comparison, we use pressure and, for the barotropic part, also the meridional velocity. Since the pressure in the LSG model was not archived, it had to be estimated from the yearly averaged barotropic and bar-
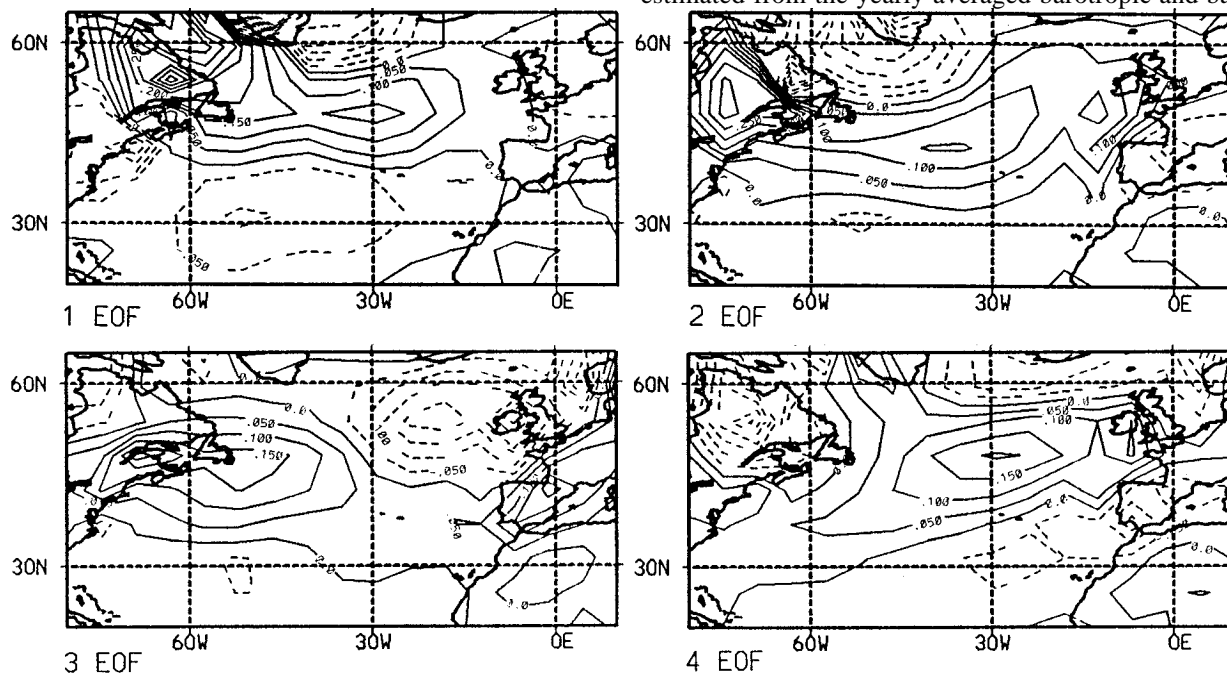

FIG. 5. First four EOFs of the ECHAM1/LSG North Atlantic wind stress curl based on yearly data from year 9 to 333, in arbitrary units. They represent 17%, 10%, 8%, and 8% of the variance.
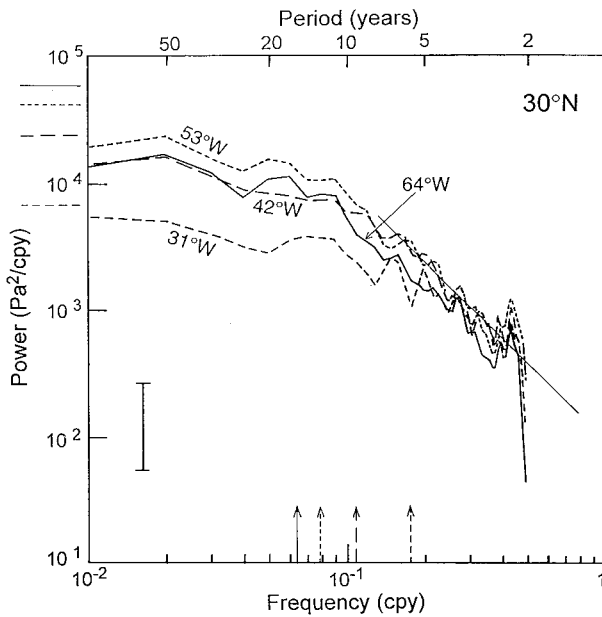
FIG. 6. Frequency spectrum of the ECHAM1/LSG baroclinic pressure at 250 m and 30°N for various longitudes. The spectra were estimated as in Fig. 4. The model predictions for the parameters listed in Table 1 are given in thin line for the high-frequency slope, the zero frequency power, and the value of ω^*, which is indicated by an arrow. The 95% confidence interval is indicated.

oclinic horizontal velocities, which were archived. This was done by a least squares fit in the North Atlantic basin, assuming geostrophy and the vanishing of the pressure at the oceanic boundaries, as in (4) and (5). Geostrophy should be a good approximation except near the boundaries, where horizontal mixing plays a role.

1) BAROCLINIC VARIABILITY

East of the Gulf Stream, the frequency spectra of the yearly baroclinic pressure fluctuations p_{bc} have a shape throughout the subtropical gyre consistent with our predictions. As illustrated in Fig. 6, the power decreases as ω^{-2} at high frequency with a level that does not depend on the longitude and it flattens at low frequency at a level that increases with the distance from the eastern boundary. A quantitative comparison requires specification of the adjustable parameters that enter (16). For the theoretical predictions in Fig. 6 we have chosen the values listed in Table 1, which we regard as physically reasonable, although a perhaps even more optimal agreement could have been obtained by tuning. East of the Gulf Stream these values nicely reproduce the spectral level at high frequencies, as well as the zonal variations in ω^* and zero frequency spectral level. To document more precisely the zonal changes, Fig. 7 (bottom) shows the p_{bc}-power in three frequency bands centered around 0.05, 0.1, and 0.2 cpy as a function of longitude. In each case the power rapidly increases with increasing distance from the eastern boundary, peaks, and then
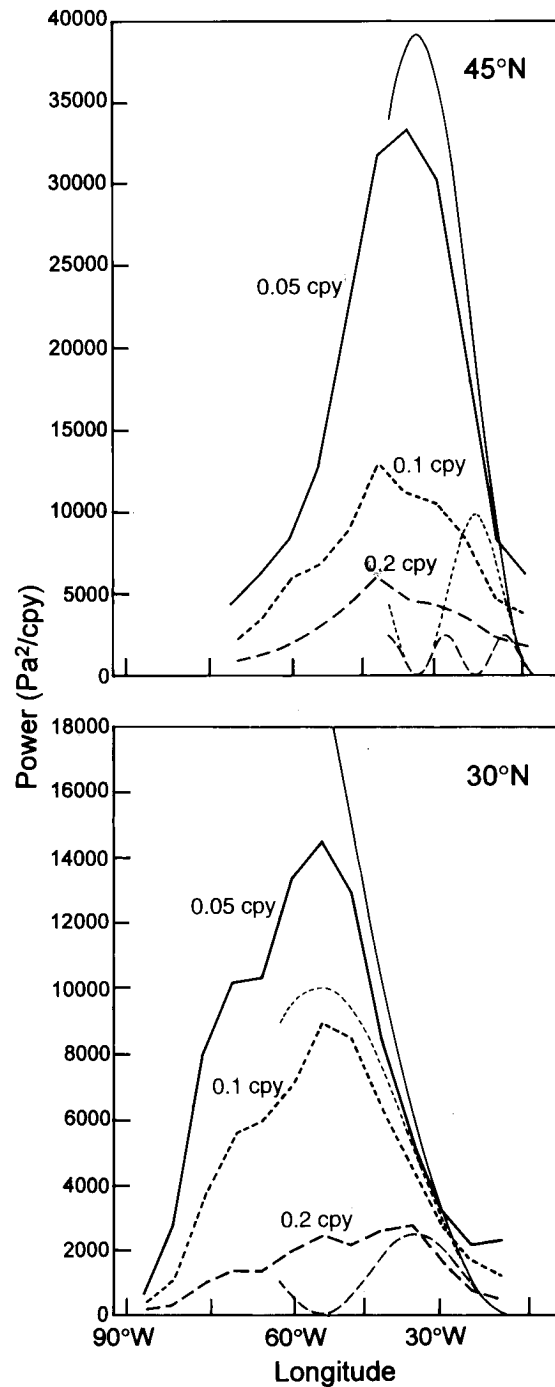
FIG. 7. Power of the ECHAM1/LSG baroclinic pressure (in Pa^2/cpy) at 250 m, 45°N (top) and 30°N (bottom) versus longitude in three frequency bands centered around 0.05, 0.1, and 0.2 cpy. The power was estimated as in Fig. 4 with a 0.03 cpy bandwidth. The model predictions are given in thin lines.

decreases westward. The agreement with the model predictions is very good at 0.2 and 0.1 cpy, while at 0.05 cpy the predicted peak is three times too high and is found much farther westward (near 90°W). However, just west of the location of the observed peak the mean

zonal current becomes large and eastward in the coupled model (see Fig. 3), so it opposes the Rossby wave speed and invalidates our simple model, which ignores any mean flow. For the baroclinic response, the effective width of the basin in the subtropical gyre is smaller than the value of Δx at 0.05 cpy.

In the model subpolar gyre, the mean currents are generally strong (see Fig. 3), so a theory for a resting ocean is less likely to apply. The predictions at 45°N are indeed not as good, as can be seen in Fig. 7 (top). The maximum power in the three frequency bands is not inconsistent with the predictions, and the location of the peak is good at 0.05 cpy. However, at 0.1 and 0.2 cpy the peaks are found much more westward than predicted. In fact, the three maxima occur at about the same longitude, which is also where the barotropic energy peaks (Fig. 9 below).

2) BAROTROPIC VARIABILITY

East of the Gulf Stream in the subtropical gyre, the barotropic meridional velocity varies coherently and nearly in phase with the wind stress curl, as predicted, and its power spectrum is modulated by the local changes of S_0 (Fig. 8, bottom). However, instead of being white as predicted, the barotropic frequency spectra are slightly red and there is more power at low frequency than expected from (1). This might be due to a coupling with the baroclinic mode, which is expected from the JEBAR effect in a stratified ocean with topography. Quantitative estimates are, however, difficult since JEBAR depends on the bottom flow that crosses f/H contours. Note that in the model Gulf Stream (at 62°W), the barotropic meridional velocity spectrum is one order of magnitude larger than within the subtropical gyre. As shown in Fig. 9 (bottom), the p_{bt}-power at the three decadal frequencies reflects the slight redness of the barotropic spectra, but increases rapidly with the distance from the eastern boundary, as in (15), peaking much farther westward than in the baroclinic case, in fact close to the western boundary. At 0.2 cpy the predicted increase is somewhat steeper and the energy level somewhat lower than in the GCM. Taking into account the zonal depth changes and the wind stress curl forcing at smaller scales would improve the agreement, but the power would remain underpredicted at the lower frequencies. As predicted, the barotropic power is smaller than the baroclinic one.

In the subpolar gyre at 45°N, the frequency spectrum of the barotropic meridional velocity in the east is also consistent with the quasi-stationary Sverdrup balance, except again for a slight redness that increases toward the west (Fig. 8, top). Note that the barotropic pressure fluctuations are comparable to the baroclinic ones. The predicted quadratic p_{bt}-power increase with the distance from the eastern boundary is nicely observed as far as 42°W, but the power in the GCM is again too large at low frequencies (Fig. 9, top). In the eastern part of the
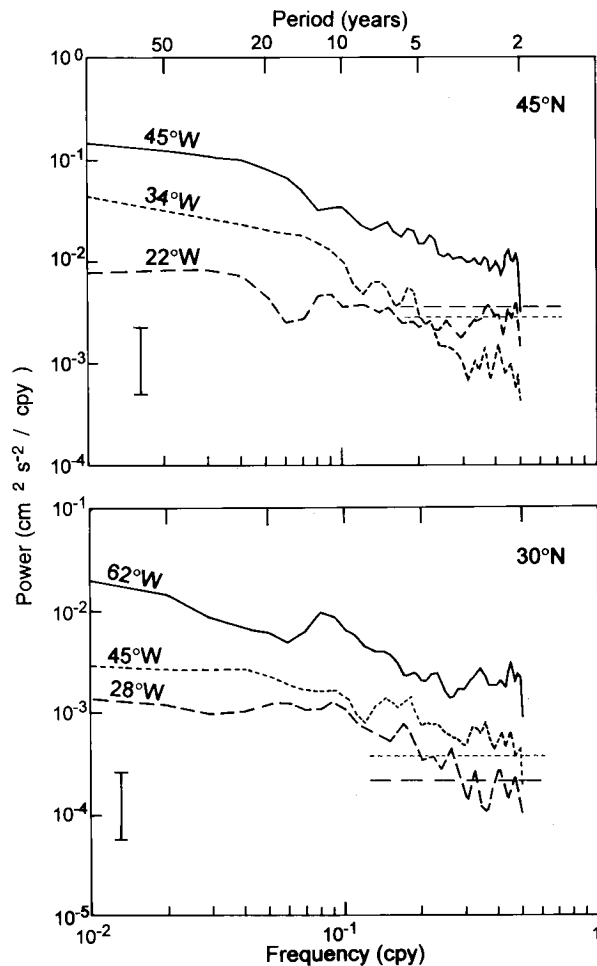

FIG. 8. Frequency spectrum of the ECHAM1/LSG barotropic meridional velocity at 45°N (top) and 30°N (bottom) for various longitudes. The spectra were estimated as in Fig. 4. The predicted spectral levels are indicated by a horizontal line for the two locations to the east of the strongest mean currents.

basin, the meridional velocity varies in phase with the wind stress curl, while in the return flow (at 45°W) it has enhanced power and is nearly out of phase, although less coherent, with the wind stress curl (Fig. 10).

d. Discussion

Our simple linear theory suggests that much of the coupled model decadal variability in the North Atlantic pressure field is directly forced by the wind via Ekman pumping. Since the wind stress curl spectrum is essentially white at low frequencies, the atmospheric forcing is stochastic and reflects the white noise extension of the short timescale weather fluctuations. The decadal variability is primarily baroclinic in the subtropical gyre. In the quiet parts of the gyre, the theory predicts quite well the shape, the level, and the geographical variability of the baroclinic power spectra as resulting from the combination of local Ekman pumping and Rossby
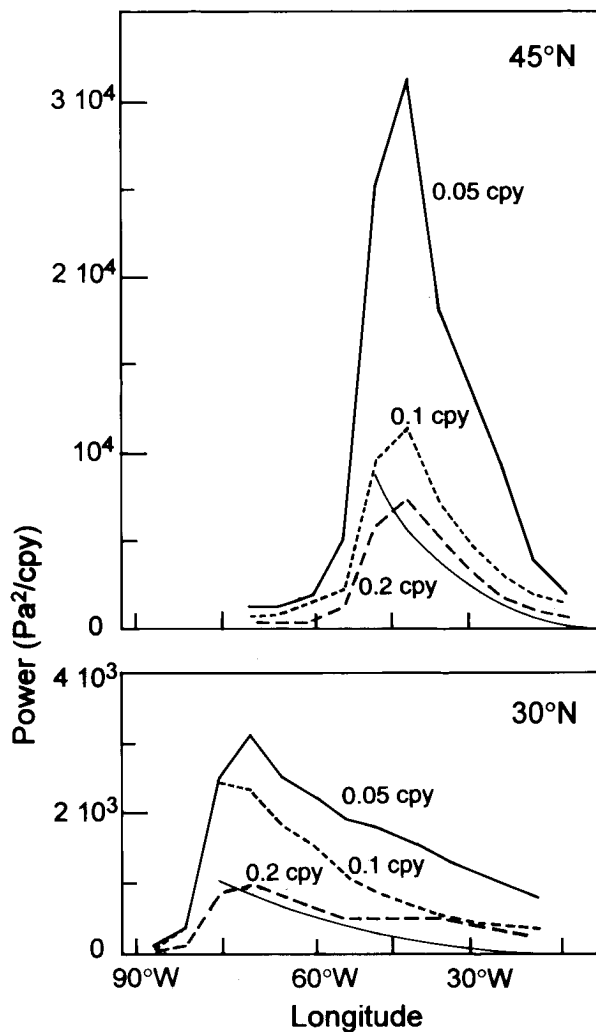
FIG. 9. Power of the ECHAM1/LSG barotropic pressure (in Pa^2/cpy) at 45°N (top) and 30°N (bottom) versus longitude in three frequency bands centered around 0.05, 0.1, and 0.2 cpy. The power was estimated as in Fig. 4 with a 0.03 cpy bandwidth. The model predictions (thin line) are for the parameters listed in Table 1.
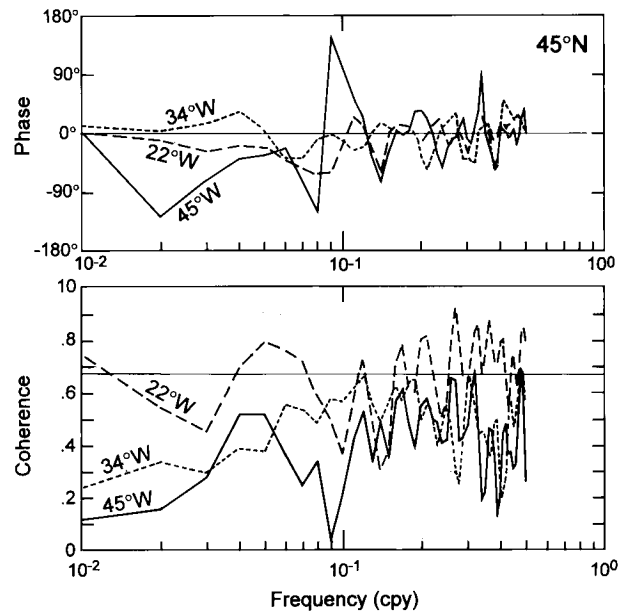

FIG. 10. Coherence (bottom) and phase (top) between the ECHAM1/LSG barotropic meridional velocity and the wind stress curl at 45°N and various longitudes. The cross spectra were estimated as in Fig. 4. The 5% level for zero coherence is indicated by a thin line.

wave propagation from the eastern boundary. However, the predictions do not hold in regions where the mean currents become comparable to the baroclinic wave speed, and a more refined model taking into account the mean flow and the associated thermocline structure needs to be considered. The barotropic fluctuations were assumed to be in time-dependent Sverdrup equilibrium, and this works fairly well throughout the subtropical gyre, even though topographic influences should be included in a more refined model. Our theory predicts that, in the easternmost part of the gyre, the baroclinic adjustment should be nearly complete at decadal frequencies, and that there should be approximate compensation at depth. Consistent with this prediction, the model deep ocean is found to be nearly at rest in the eastern part of the gyre. In the central and western parts of the gyre, however, there is insufficient time for bar-

oclinic adjustment and weak currents are found below the thermocline (not shown).

In the subpolar gyre, the barotropic response is also rather well-predicted by a time-varying Sverdrup equilibrium, at least east of the regions with the largest currents. Our theory is less successful for the baroclinic variability, presumably because the mean currents are too large and topographic influences too strong.

In their analysis of the North Atlantic decadal variability, Zorita and Frankignoul (1997, henceforth ZF) found substantial temperature fluctuations in and above the thermocline, with a spectrum comparable to those in Fig. 6. The variability appeared to be atmospherically forced, and at depth temperature and salinity were changing in phase, as expected from vertical or horizontal thermocline displacements, with opposite sign in the subtropical and subpolar gyres. Here we showed that the ocean interior is primarily reflecting the first baroclinic mode response to stochastic Ekman pumping, the meridional scale being set by that of the forcing, which tends to have opposite signs in the two gyres (see Fig. 5). Using extended empirical orthogonal function analysis, ZF identified two distinct quasi-oscillatory modes of ocean–atmosphere variability with a dominant period of about 20 and 10 years. In the two modes, the oceanic changes seemed to be forced by the atmosphere via air–sea fluxes and Ekman pumping, which after some delay affected the intensity of the gyres. The more energetic 20-yr mode of ZF was easily seen in the thermocline but was not found in the atmosphere alone, thereby reflecting a passive oceanic response, but what deter-

mines its dominant timescale could not be established. Our analysis suggests that it is given by the time it takes a long baroclinic Rossy wave to propagate across the effective width of the basin so that the mode can be considered a fetch limited first baroclinic mode response. The extended EOF analysis, which acts as a narrow-band filter, isolates the most energetic fluctuations, which are around 20-yr period in both the subtropical and subpolar gyres (Fig. 6). The 10-yr mode in ZF had similar spatial scales but was less energetic and more surface trapped, and it behaved independently from the 20-yr mode. Since the mode could be detected in an extended EOF analysis of the atmosphere alone, albeit with a very small signal-to-noise ratio, it was speculated to be a coupled mode linked to some positive air–sea feedback. We could not find any evidence of a statistically significant 10-yr peak in the wind stress curl spectrum when using standard spectral analysis. Thus, the feedback must be very weak and the 10-yr mode should not be significantly more energetic in the ocean interior than expected from our stochastic forcing approach. A more refined model including mixed layer dynamics is needed to understand its surface trapping and its coupling with the atmosphere.

In the North Pacific, the air–sea feedback in coupled model simulations appears to be stronger at decadal scales (Latif and Barnett 1994; Robertson 1996). It remains to be shown what fraction of the oceanic variability can be explained by stochastic forcing.

4. Comparison with observed data

a. Wind stress curl spectrum

The wind stress curl frequency spectrum depends on the effective spatial resolution of the data. For the present purpose only scales comparable to or larger than the basin size enter the white noise level S_0.

In the North Atlantic, Mac Veigh et al. (1987) analyzed 4 years of ECMWF surface wind stress curl data estimated from surface wind analysis. Although the seasonal signal was not removed, frequency spectra representative of about 25°N and 46°N were white at periods longer than 50 days, with a white noise level of 4×10^{-16} and 4×10^{-15} (Pa m^{-1})^2/cpy, respectively, about four times more than in the ECHAM1/LSG model. The zonal wavenumber spectra were red and, correspondingly, the main wind stress curl EOFs had basin-wide zonal scales (see also Ehret and O'Brien 1989). About one-third of the above white noise levels seems to correspond to the basin scales, which set S_0.

In the North Pacific, the dominant EOFs also have a zonal scale that is larger than, or comparable with, that of the basin (Rienecker and Ehret 1988); hence our solutions for zonally independent forcing should also be relevant. Using 11 years of monthly COADS data, Gallegos-Garcia et al. (1981) computed wind stress curl spectra, which resolved wavelengths between 400 and 4000 km. The frequency spectrum for midlatitudes (29°–39°N) was white except for a small annual peak, and its level about 2×10^{-15} (Pa m^{-1})^2/cpy. The zonal wavenumber spectrum was nearly symmetric and very slightly red.

Wind stress curl spectra over the North Pacific have also been calculated from analyzed data. Chave et al. (1991) used 3 years of FNOC winds with an effective smoothing scale about 500 km. At low frequencies, the white noise level was 8×10^{-15} (Pa m^{-1})^2/cpy at 45°N, 147°W, and $6 \ 10^{-15}$ (Pa m^{-1})^2/cpy at 41°N, 162°W, with no preferred propagation direction. Large et al. (1991) considered 7 years of ECMWF analyses on a 2.5° × 2.5° grid. The white noise level was $4 \ 10^{-15}$ (Pa m^{-1})^2/cpy at 40°N, 190°E. A wavenumber–frequency spectrum at 31°N showed some redness at wavelengths larger than 1000 km, a steep fall off at shorter scales, and symmetry at low frequencies.

In summary, the spectra of the observed wind stress curl at the monthly to yearly timescale are white and symmetric as in the ECHAM1/LSG model, but there is some redness at low k and the energy levels are substantially larger. Correspondingly, the oceanic response should also be larger than in the coupled model. Whether the wind stress curl frequency spectrum remains white down to decadal frequencies is not known. Sturges and Hong's (1995) calculation based on 43 years of COADS data along 32°N in the North Atlantic suggests that it becomes red, but the redness is not statistically significant.

b. Bermuda tide gauge and temperature data

There are very few oceanic time series of measurements that are long enough to estimate power spectra at decadal frequencies. However, observations near Bermuda (32°N, 64°W) allow for a quantitative comparison with our theoretical predictions for the baroclinic response. Bermuda is just east of the western boundary current region and our simple model should hold. The fetch is larger than in the coupled model ($\Delta x = 5000$ km), and we thus expect the power spectra to peak around 0.06 cpy, which alone would lead to a much larger energy level than in Fig. 6. The wind stress curl power is also larger, which will further increase the predicted response. Lacking a direct calculation, we estimate from the values quoted above the basin-scale white noise level to be about 3×10^{-16} Pa^2 m^{-2}/cpy.

The Bermuda tide gauge record, which is nearly continuous since 1945, was analyzed by Sturges and Hong (1995) in relation to wind forcing across the Atlantic. Using the COADS data to estimate the wind stress curl and the same baroclinic mode longwave model as in (3), but with a longitudinally varying wave speed (or baroclinic depth scale) calculated from climatological hydrographic data along 32°N, they found a remarkable agreement between the observed and predicted changes at the decadal scale. As in our calculation, the sea level
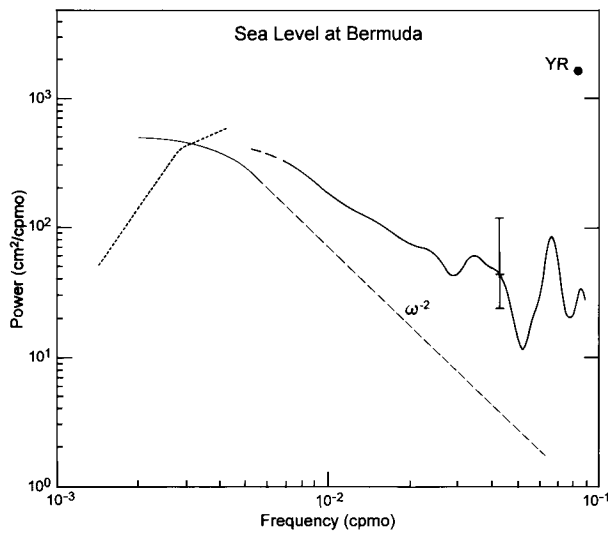
FIG. 11. Frequency spectrum of sea level at Bermuda. Thick line: Full curve shows a calculation from the continuous portion of data beginning in 1944, smoothed by three Hanning passes (the 90% confidence interval is indicated), except for the last point shown (dashed). The dotted segment at low frequencies was obtained using gappy data extending back to 1932 (after Sturges and Hong 1995). Thin line: model prediction for the low frequencies (continuous line) and the high-frequency slope (dashed line).
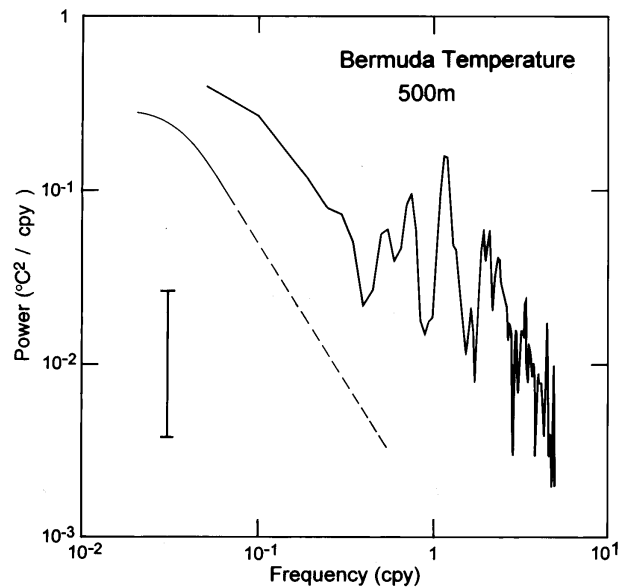

FIG. 12. Frequency spectrum of 500-m temperature at Bermuda. Thick line: Panulirus data (the spectrum was estimated with the Tukey method and the 95% confidence interval is indicated). Thin line: model prediction for the low frequencies (continuous line) and the high-frequency slope (dashed line).

was affected by the local and the remote response to Ekman pumping. Figure 11 reproduced from Sturges and Hong shows the sea level frequency spectrum to be red, decaying approximately as $\omega^{-1.5}$ at periods less than 200 mo (the high frequency whitening is due to data noise). Using earlier data to extend the time series, Sturges and Hong (1995) speculated that the spectrum would peak at a period shorter than 500 mo, and they suggested that this was due to the limited basin width. Clearly, this deterministic simulation makes a very convincing case for the importance of wind stress curl forcing at the decadal scale. To compare the observed spectrum with our prediction for stochastic forcing, we approximate the sea level by $\eta = p_{bc}(0)/\rho g$, since the barotropic contribution should be smaller than the baroclinic one [see (20)]. The prediction (16) calculated with the values from Table 1 matches well the observed energy level at the decadal scale, while having a slightly steeper slope at higher frequencies, presumably because it is not contaminated by data and eddy noise. The good agreement confirms that the flattening at low frequencies is due to the limited distance to the eastern boundary. It also suggests that there may be no need to invoke, as in Sturges and Hong (1995), a strong hypothetical redness of the wind stress curl at the lowest frequencies to explain the sea level spectrum: our estimated white noise level already provides consistent predictions.

Joyce and Robbins (1996) analyzed 36 years of nearby hydrographic stations made by the R. V. *Panulirus*, which showed large interannual and decadal variations in temperature and salinity. In the thermocline, the de-

cadal temperature and salinity anomalies were highly correlated, suggesting vertical or meridional displacements, while at deeper levels the changes appeared to be unrelated. The temperature changes in the thermocline can be compared to our predictions for baroclinic fluctuations. If one assumes for simplicity that they are due to vertical motions, one has

$$T = \frac{d\bar{T}/dz}{g d\bar{\rho}/dz} p_{bc} \frac{d\phi}{dz}. \qquad (21)$$

For the parameters listed in Table 1 this prediction is shown in Fig. 12. Our model matches well the very low-frequency energy level, while underestimating the temperature spectrum by a factor of 2 or 3 at the decadal scale (Fig. 12). The excess energy in the Bermuda observations at high frequency is likely to be due to eddy contamination (Frankignoul 1981) and data noise.

In summary, our simple model suggests that the decadal variability at Bermuda is to a large extent due to stochastic wind stress forcing. Whether our slight underestimation of the observed spectra can be attributed to poor parameter choices and our disregard of the wind stress curl forcing on scales smaller than the basin remains to be established.

5. Conclusions

In this paper we have used a simple linear stochastic forcing model to explain the decadal variability in certain regions of the extratropical ocean. Because of their fast adjustment time, the barotropic fields were assumed to be governed at decadal timescales by a time-dependent

Sverdrup balance where the input of vorticity by the wind is instantaneously balanced by a change in planetary vorticity. The baroclinic variability was modeled by the equation for long nondispersive Rossby waves forced by wind stress curl fluctuations. The wind stress forcing was assumed to be stochastic with a white frequency spectrum, so the oceanic response represents the continuous excitation of the ocean interior by short timescale weather fluctuations. The model was further simplified by using a radiation condition in the west and by assuming a flat bottom, a mean state that is at rest, zonally independent forcing, and no dissipation. At each frequency, the baroclinic response consists of a forced response plus a Rossby wave generated at the eastern boundary. For zonally independent forcing, the response propagates westward at twice the Rossby phase speed, which might account for the hitherto unexplained faster phase speed of the Rossby waves observed in upper thermal data and in altimetric observations. Our analysis is statistical. The model predicts the shape and level of the frequency spectra and their variation with longitude and latitude.

The model predictions were compared with the variability found in the North Atlantic pressure field in an extended integration of the ocean–atmosphere ECHAM1/ LSG coupled GCM. It is surprising how much of this variability can be reproduced by our analytical model, given its extreme simplicity. Specifically, our model predicts a red baroclinic spectrum with a high-frequency ω^{-2} decay that levels off at low frequency to a constant value. This is also the shape seen in the GCM spectra. Furthermore, our theory correctly predicts how this spectral shape changes with longitude as a result of the varying fetch and with latitude as a result of changes in the Coriolis parameter, the stratification, and the forcing level. Although the baroclinic response is spread over a continuum of frequencies, it can be associated with a dominant timescale that is given by the time it takes a long baroclinic Rossby wave to propagate across the basin and that increases with the effective width of the basin. Our model predicts that the barotropic frequency spectra are white, whereas the GCM spectra are slightly red. Nevertheless, the theory captures correctly how the barotropic pressure spectra vary with longitude, latitude, and wind stress field intensity. The good agreement is mostly confined to the interior of the subtropical gyre and, to a lesser extent, the subpolar gyre. This is a comparatively small area in the coupled GCM since its Gulf Stream is broad and shifted southeastward. However, our baroclinic predictions for a white wind stress curl spectrum are also broadly consistent with the shape and level of the frequency spectrum of sea level and temperature measured in the thermocline near Bermuda, which suggests that our model is also an appropriate starting point for understanding decadal changes in the real ocean.

Although our model is successful in the gyre interiors, closer inspection and comparisons reveal various discrepancies. However, a model as coarse as ours cannot be expected to reproduce details. It is anticipated that improvements would be obtained by including topography and a realistic basic state, and by considering a more realistic forcing. In particular, we speculated that the interaction of baroclinic currents with topography (via JEBAR) is the reason for the redness of the barotropic spectra in the GCM. Realistic basic states have a non-uniform thermocline structure and often have a mean current that is comparable to the phase speed of the baroclinic Rossby waves, which would also lead to modifications of the model predictions. Though the atmospheric forcing has large zonal scales, it is not independent of the zonal coordinate as assumed here; hence the use of a more realistic wind stress curl spectrum should similarly improve our predictions. Also, considering the meridional structure of the wind stress curl forcing would allow one to look at the evolution of the spatial patterns in time, as analyzed in coupled models.

The comparison has been limited to the North Atlantic, due to data availability, but will be extended in future work to the North Pacific. Overall, the present results suggest that our stochastic forcing model can serve as a zeroth-order model for the decadal variability of the pressure field and the associated geostrophic velocity field in the interior of the gyres. Whether or not a substantial part of the sea surface temperature variations at decadal frequencies can be explained by the associated modulation of the surface mixed layer remains to be evaluated.

APPENDIX

Baroclinic Response to x-Dependent Forcing

The baroclinic response to *x*-dependent forcing is given by (7). For a single spatial Fourier component $\hat{F}(x, \omega) = \hat{F}(\omega)e^{ikx}$, the response is given by

$$\hat{p}_{bc}(x,\,\omega) = \frac{H}{\beta H_{bc}} \frac{1}{i(k_{bc} - k)}(e^{ik_{bc}x} - e^{ikx})\hat{F}(\omega) \quad (A1)$$

and again consists of a directly forced part with wavenumber k and a remotely forced Rossby wave with wavenumber k_{bc}. In this case, the propagation speed of the response is wavenumber dependent and given by $2\omega/(k + k_{bc})$. For forcing scales much larger than that of the Rossby wave, it is still about twice larger than

for a free wave. In case of resonance, $k = k_{bc}$, the response grows linearly in x away from the eastern boundary and propagates at the Rossby wave speed. Other spatial patterns can be obtained by adding their Fourier components. In particular, the response to a standing forcing pattern, $\hat{F}(x, \omega) = \hat{F}(\omega)\cos(kx - \phi)$, is given by

$$
\hat{p}_{bc}(x, \omega) = \frac{1}{2}\frac{H}{\beta H_{bc}}\left[\frac{1}{i(k_{bc} - k)}(e^{ik_{bc}x} - e^{ikx})e^{-i\phi}\right.
$$

$$
\left. + \frac{1}{i(k_{bc} + k)}(e^{ik_{bc}x} - e^{-ikx})e^{i\phi}\right]\hat{F}(\omega).
\tag{A2}
$$

REFERENCES

Bjerknes, J., 1964: Atlantic air–sea interactions. *Advances in Geophysics,* Vol. 10, Academic Press, 1–82.

Chave, A. D., D. S. Luther, and J. H. Filloux, 1991: Variability of the wind stress curl over the North Pacific: Implication for the oceanic response. *J. Geophys. Res.,* **96,** 18 361–18 379.

Chelton, D. B., and M. G. Schlax, 1996: Global observations of oceanic Rossby waves. *Science,* **272,** 234–238.

Cubasch, U., K. Hasselmann, H. Hoeck, E. Maier-Reimer, and U. Mikolaewicz, 1992: Time dependent greenhouse warming computation with a coupled ocean–atmosphere model. *Climate Dyn.,* **8,** 55–69.

Delworth, T., S. Manabe, and R. Stouffer, 1993: Interdecadal variability of the thermohaline circulation in a coupled ocean–atmosphere model. *J. Climate,* **6,** 1993–2011.

Deser, C., and M. L. Blackmon, 1993: Surface climate variations over the North Atlantic Ocean during winter 1900–1989. *J. Climate,* **6,** 1743–1753.

Ehret, L. L., and J. J. O'Brien, 1989: Scales of North Atlantic wind stress curl determined from the comprehensive ocean–atmosphere data set. *J. Geophys. Res.,* **94,** 831–841.

Frankignoul, C., 1981: Low-frequency temperature fluctuations off Bermuda. *J. Geophys. Res.,* **86,** 6522–6528.

——, 1995: Climate spectra and stochastic climate models. *Analysis of Climate Variability. Application of Statistical Techniques,* H. von Storch and A. Navarra, Eds., Springer-Verlag, 29–51.

Gallegos-Garcia, A., W. J. Emery, R. O. Reid, and L. Magaard, 1981: Frequency-wavenumber spectra of sea surface temperature and wind-stress curl in the eastern Pacific. *J. Phys. Oceanogr.,* **11,** 1059–1077.

Gates, W. L., U. Cubasch, G. A. Meehl, J. B. Mitchell, and R. Stouffer, 1993: An intercomparison of selected features of the control climates simulated by coupled ocean–atmosphere general circulation models. Report of the Steering Group on Global Climate Modelling, WMO/TD. 51 pp. [Available from WMO, CP 2300, CH-1211, Geneva 2, Switzerland.]

Graham, N. E., 1994: Decadal-scale climate variability in the tropical and North Pacific during the 1970s and 1980s: Observations and model results. *Climate Dyn.,* **10,** 135–162.

Hasselmann, K., 1976: Stochastic climate models. Part I: Theory. *Tellus,* **28,** 473–485.

Joyce, T. M., and P. Robbins, 1996: The long-term hydrographic record at Bermuda. *J. Climate,* **9,** 3121–3131.

Kessler, W. S., 1990: Observations of long Rossby waves in the northern tropical Pacific. *J. Geophys. Res.,* **95,** 5183–5217.

Kushnir, Y., 1994: Interdecadal variations in North Atlantic sea surface temperature and associated atmospheric conditions. *J. Climate,* **7,** 141–157.

Lagerloef, G. S. E., 1995: Interdecadal variations in the Alaska gyre. *J. Phys. Oceanogr.,* **25,** 205–213.

Large, W. G., W. R. Holland, and J. C. Evans, 1991: Quasi-geostrophic ocean response to real wind forcing. *J. Phys. Oceanogr.,* **21,** 998–1017.

Latif, M., and T. P. Barnett, 1994: Causes of decadal climate variability in the North Pacific/North American sector. *Science,* **266,** 634–637.

Levitus, S., 1989: Interpentadal variability of temperature and salinity at intermediate depths of the North Atlantic Ocean, 1970–74 versus 1955–59. *J. Geophys. Res.,* **94,** 6091–6131.

——, J. I. Antonov, and T. P. Boyer, 1994: Interannual variability at a depth of 125 meters in the North Atlantic Ocean. *Science,* **266,** 96–99.

Liu, Z., 1993: Thermocline forced by varying Ekman pumping. Part II: Annual and decadal Ekman pumping. *J. Phys. Oceanogr.,* **23,** 2523–2540.

Mac Veigh, J. P., B. Barnier, and C. Le Provost, 1987: Spectral and empirical orthogonal function analysis of four years of European Center for Medium Range Weather Forecast wind stress curl over the North Atlantic Ocean. *J. Geophys. Res.,* **92,** 13 141–13 152.

Maier-Reimer, E., U. Mikolajewicz, and K. Hasselmann, 1993: Mean circulation of the Hamburg LSG OGCM and its sensitivity to the thermohaline surface forcing. *J. Phys. Oceanogr.,* **23,** 731–757.

Rienecker, M. M., and L. L. Ehret, 1988: Wind stress curl variability over the North Pacific from the Comprehensive Ocean–Atmosphere Data Set. *J. Geophys. Res.,* **93,** 5069–5077.

Robertson, A. W., 1996: Interdecadal variability over the North Pacific in a coupled ocean–atmosphere general circulation model. *Climate Dyn.,* **12,** 227–241.

Roeckner, E., K. Arpe, L. Bengtsson, S. Brinkop, L. Dümenil, M. Esch, E. Kirk, F. Lunkheit, M. Ponater, B. Rockel, R. Sausen, U. Schlese, S. Schubert, and M. Windelband, 1992: Simulation with the present day climate with the ECHAM model: Impact of model physics and resolution. Max-Planck-Institut für Meteorologie Rep. No. 93, Hamburg, Germany, 171 pp. [Available from MPI, Bundestrasse 55, D-20146 Hamburg, Germany.]

Sturges, W., and B. G. Hong, 1995: Wind forcing of the Atlantic thermocline along 32°N at low frequencies. *J. Phys. Oceanogr.,* **25,** 1706–1715.

Trenberth, K. E., and J. Hurrell, 1994: Decadal atmosphere–ocean variations in the Pacific. *Climate Dyn.,* **9,** 303–319.

von Storch, J., 1994: Interdecadal variability in a global coupled model. *Tellus,* **46A,** 419.

White, W. B., 1977: Annual forcing of baroclinic long waves in the tropical North Pacific Ocean. *J. Phys. Oceanogr.,* **7,** 50–61.

——, 1985: The resonant response of interannual baroclinic Rossby waves to wind forcing in the eastern midlatitude North Pacific. *J. Phys. Oceanogr.,* **15,** 404–415.

Zhang, Y., J. M. Wallace, and N. Iwasaka, 1996: Is climate variability over the North Pacific a linear response to ENSO? *J. Climate,* **9,** 1468–1478.

Zorita, E., and C. Frankignoul, 1997: Modes of North Atlantic decadal variability in the ECHAM1/LSG coupled ocean–atmosphere general circulation model. *J. Climate,* **10,** 183–200.